Journal of ELECTRONIC MATERIALS, Vol. 38, No. 4, 2009
DOI: 10.1007/s11664-008-0612-3

Current-Induced Degradation of Nickel Ohmic Contacts to SiC

B.P. DOWNEY,[1] J.R. FLEMISH,[1,2,4] B.Z. LIU,[3] T.E. CLARK,[3] and S.E. MOHNEY[1,3,5]

1.—Department of Materials Science and Engineering, The Pennsylvania State University, University Park, PA 16802, USA. 2.—Applied Research Laboratory, The Pennsylvania State University, University Park, PA 16802, USA. 3.—Materials Research Institute, The Pennsylvania State University, University Park, PA 16802, USA. 4.—e-mail: jflemish@psu.edu 5.—e-mail: mohney@ems.psu.edu

The stability of Ni ohmic contacts to *p*-type SiC under high current density was investigated. A test structure adapted from the four circular contacts method allowed for vertical stressing and the ability to extract a pre- and post-stressed specific contact resistance. The accuracy of the measured specific contact resistance was verified experimentally through comparisons with more widely used methods and the use of computer modeling. The growth of voids initially produced during the high-temperature ohmic contact anneal was found to be the degradation mechanism, effectively decreasing the area of the contact.

Key words: Ohmic contact, SiC, reliability, current stress, contact resistance, nickel

INTRODUCTION

The decreased scaling of dimensions coupled with the integration of wide-bandgap semiconductor materials for high-power applications will continue to increase the operating current density of electronic devices. One area of concern that stems from higher current densities is the susceptibility of ohmic contacts to degradation via electromigration or reactions produced by Joule heating. Understanding the possible degradation mechanisms in each metal/semiconductor system is important in order to engineer more stable ohmic contacts. The reliability of contacts to Si on the order of a micron or less utilizing various metallization schemes for integrated circuit (IC) technology has been studied.[1–7] The findings illustrate the potential for reactions and diffusion between the metals and the semiconductor, causing an increase in resistance, leading to thermal runaway, as well as the movement of material away from the contact interface, producing an open circuit. The degradation mechanisms varied depending on the metallization used.

(Received September 3, 2008; accepted December 1, 2008; published online January 24, 2009)

Wide-bandgap semiconductors should also be investigated separately, as new degradation mechanisms may be present in different material systems. SiC is a candidate for such a study because of its use in high-temperature, high-power electronics.[8] One of the most common and highly researched metals used to form an ohmic contact to SiC is Ni.[9–11] While Ni is typically used as a contact to *n*-type SiC, it has also been demonstrated for use as a contact to *p*-type SiC.[12,13] Although Ni has shown the ability to provide a low specific contact resistance to SiC, the reaction products of the necessary high-temperature anneal, including carbon segregation during nickel silicide formation, have the potential to cause reliability problems.[14–16]

This paper will examine the stability of Ni ohmic contacts to SiC under high current density. The aforementioned reliability studies of contacts to Si were performed by stressing two contacts laterally through an implanted layer, typically using a cross-bridge Kelvin resistor structure to measure the specific contact resistance. In this study, contacts are stressed vertically through a PiN diode structure to emulate the current flow in a vertical device. A test structure derived from the four circular contacts method (FCCM)[17] is used to vertically stress small contacts to *p*-type SiC, while being able to

extract pre- and post-stressed values of specific contact and semiconductor sheet resistance using a lateral technique. A metallization scheme that includes the annealed Ni ohmic contact, a TiW diffusion barrier, and a thick electroplated Au overlayer is used to simulate a power device. DC current densities above 10^5 A/cm^2 are used to stress the contacts to failure. Failure analysis was performed using field-emission scanning electron microscopy (FESEM) of the surface of the samples and cross sections prepared using a focused ion beam (FIB), as well as Auger electron spectroscopy (AES). Additionally, the validity of the FCCM structure was verified by a comparison with the widely used transfer length method (TLM)[18] and circular transfer length method (CTLM)[19] test structures. Simulations of the FCCM using Sentaurus Structure Editor and Device by Synopsys were also employed to examine the legitimacy of the method.

EXPERIMENT

The SiC PiN diode structure was obtained from Cree, Inc., and consisted of epilayers grown on a research-grade n-type 4H substrate cut 8 deg off [0001] and doped to 1×10^{18} cm^{-3}. On top of the substrate, a 10-μm n^- drift layer was grown with a donor density of 2×10^{14} cm^{-3}, followed by a 2.5-μm p-type injection layer doped at 8×10^{18} cm^{-3} and a 0.5-μm p^{++} capping layer doped to 1×10^{20} cm^{-3}. The samples were initially cleaned using a standard Radio Corporation of America (RCA) process.[20] The FCCM test structure is based on the four-point probe method and requires four equally spaced circular contacts deposited on a rectangular isolated semiconductor layer. Current is forced through the outer contacts while the inner contacts are used to measure a voltage drop across the semiconductor to determine a sheet resistance. Then the specific contact resistance can be extracted for the outer contacts by measuring the voltage drop across those contacts for the same applied current, requiring only two measurements. Further details on the derivation of the method can be found in the FCCM reference.[17] Similar to the TLM approach, a mesa isolation step is needed to fabricate the structure. Because of the small contacts used in this study, larger Au bond pads are integrated into the process to probe the contacts, so two additional steps are required to facilitate contact stressing and measuring the contact resistance. An insulating layer of silicon nitride (SiN_x) separates the bond pads from the SiC. Vias are etched in the SiN_x in order for the bond pads to make electrical connection to the ohmic contacts. A schematic of the final structure is illustrated in Fig. 1.

Mesas for the FCCM and TLM structures were formed on the p-type side by inductively coupled plasma reactive-ion etching (ICP-RIE) using indium tin oxide (ITO) as an etch mask, which was patterned via photolithography and liftoff. The ITO

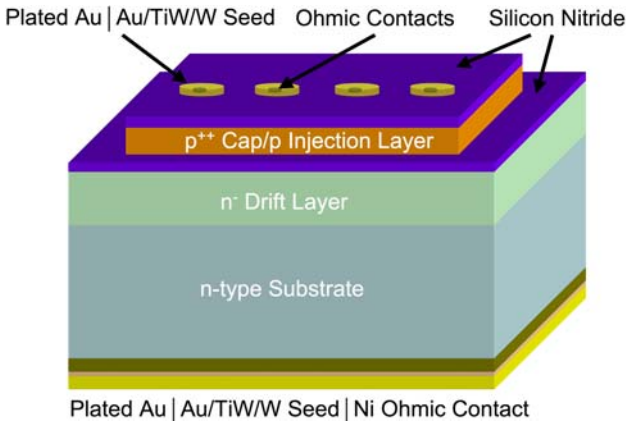

Fig. 1. Illustration of the final adapted FCCM structure.

was deposited by DC magnetron sputtering using Ar and removed using a dilute HCl solution. The mesas were etched through the p-type layers using a chemistry containing CF_4 and O_2, and isolation was verified electrically after etching. The samples were degreased in acetone, isopropanol (IPA), and deionized (DI) water and were then blown dry with N_2. Next they were subjected to 10:1 NH_4F:HF buffered oxide etch (BOE) to remove any oxide. Samples were then rinsed in DI water, dried with N_2, and immediately loaded into a deposition chamber. A blanket contact was made to the back, n-type side with 150 nm of Ni using DC magnetron sputtering at 5 mTorr. The contacts were annealed at 1000°C for 60 s using a rapid thermal annealing furnace (RTA) under flowing Ar. The samples were again degreased and patterned to define the ohmic contacts for the different test structures on the p-type side. After a 2-min 10:1 BOE soak, DI water rinse, and N_2 dry, Ni contacts were deposited using DC magnetron sputtering at 5 mTorr to a thickness of 100 nm. Following metal liftoff, the contacts were annealed in an RTA at 800°C for 60 s in Ar.

A 100-nm blanket layer of SiN_x was deposited on the p-type side by plasma-enhanced chemical vapor deposition (PECVD) using a ratio of NH_3 to SiH_4 of 10:1. Vias in the SiN_x to the ohmic contacts were formed by reactive-ion etching (RIE) using patterned photoresist as an etch mask and CF_4/O_2 as an etching chemistry, followed by removal of the photoresist. A TiW diffusion barrier and Au seed layer for electroplating were then blanket-deposited on each side of the samples by DC magnetron sputtering. The deposition sequence was the following: 10 nm of W was deposited before 60 nm of TiW sputtered from a 90 wt.% W target, followed by 100 nm of Au. The p-type side was patterned to form 75-μm-radius bond pads above the contacts used in the FCCM structures and allow for the TLM and CTLM structures to employ the same metallization scheme on other parts of the sample. The Au overlayer was deposited by pulsed DC electroplating, using Techni Gold 25 ES solution by Technic, Inc.,

to a thickness of greater than 1.5 μm, as measured using a profilometer. A DC bias was pulsed at 10 Hz with a duty cycle of 0.5 for 1 h with a peak current density of 1 mA/cm^2. The samples were placed in the bath with the p-type side facing the anode plate. After photoresist removal, the Au was etched back to remove the seed layer via RIE using a mixture of Cl_2, CF_4, and Ar followed by a quick dip in Transene GE-8148 Au etch to remove any Au redeposited during dry etching. The exposed TiW and W layers were removed using hydrogen peroxide (H_2O_2, 30%).

Specific contact and sheet resistance measurements made by the FCCM used a current of 0.1 mA to avoid stressing the contacts. All electrical measurements and stressing were performed using a Keithley 4200 SCS and probe station. FCCM geometries included structures with a mesa size of 1000 μm $\times$ 300 μm with 200 μm between the centers of each contact and a 1500 μm $\times$ 400 μm mesa with 300 μm between contacts. The middle voltage probe contacts had a radius of 10 μm to limit current shunting through the contacts, while the outer contacts had a radius of 10 μm, 20 μm, 40 μm or 60 μm. One of the outer contacts was used for current stressing. Prestressed contact resistance measurements were then compared with TLM and CTLM results. In order to obtain high enough current densities to cause degradation, only the 10-μm outer contacts were used for current stressing. Constant current ranging from 400 mA to 750 mA, corresponding to current densities of 1.27×10^5 A/cm^2 to 2.39×10^5 A/cm^2, was applied to one of the outer contacts with the positive bias on the p-type side and the n-type side grounded. The stressing was performed in ambient at room temperature for 1 h. Since the FCCM uses both outer contacts in the determination of specific contact resistance, it is assumed that the unstressed outer contact was not affected by the current stressing for post-stressed measurements. FESEM of the surface and cross sections of the contacts was performed using a LEO 1530 FESEM. Cross sections of contacts were prepared by a FEI Quanta 200 3D Dual-Beam FIB using Ga ions and selectively patterning a W protective layer to protect the areas of interest. Elemental analysis was done on the Ni/SiC reaction region using a PHI 670 field-emission scanning Auger microprobe after wet etching the above layers. The Au overlayer was etched with Transene GE-8148, the TiW and W layers were etched in H_2O_2 for 5 min, and the SiN_x was etched using a 10:1 DI H_2O:HF solution for 45 s.

FCCM SIMULATIONS

Validation of the FCCM was necessary as prestressed contact measurements exhibited a dependence of specific contact resistance on outer contact radius, with an increase in contact radius leading to an apparent increase in specific contact resistance, as shown in Table I. Semiconductor sheet resistance and specific contact resistance values extracted by the FCCM, CTLM, and TLM were therefore compared. The discrepancy between the semiconductor sheet resistance determined by the CTLM and TLM can be attributed to the contact width in the TLM structure not exactly matching the width of the mesa, which was confirmed using the same modeling approach as for the FCCM described subsequently. For the FCCM, while all the contact sizes showed little variation in measured sheet resistance, which compared well with the CTLM and TLM results, only the 10-μm-radius contact exhibited good agreement of specific contact resistance with the other methods. There was no obvious variation in specific contact resistance due to the two different mesa geometries described previously for the FCCM. However, as the contact size decreases, the extracted specific contact resistance approaches that measured by the TLM and CTLM. To further investigate this phenomenon, Sentaurus Structure Editor and Device by Synopsys, version Z-2007.03, were used to create a similar FCCM structure and simulate its electrical characteristics. A rectangular SiC slab was used in the model with dimensions of 1000 μm long by 300 μm wide, the same dimensions as one of the fabricated mesas. The simulated thickness of the slab was 0.5 μm, matching that of the p^{++} layer, since simulations showed an order of magnitude more current in that layer compared with the 2.5 μm p-type layer beneath it. The doping density of the 0.5-μm layer was adjusted until the calculated sheet resistance from the simulations was close to the experimental value. The final doping density used in the simulations reflected a sheet resistance of 321 $\Omega/\square$, which was consistent throughout all the simulations. Two metal cylinders with varied radii and height of 1 μm were used as the contacts and placed exactly where the outer contacts in the fabricated FCCM structure would be located (centers were 200 μm from the short edge of the slab). The electrical properties of Au were used

Table I. Comparison of Specific Contact and Sheet Resistance from the CTLM, TLM, and FCCM Measurements Using Different Contact Sizes

	ρ_c (Ω cm^2)	R_s ($\Omega/\square$)
CTLM	$(2.1 \pm 1) \times 10^{-5}$	331 ± 50
TLM	$(3.0 \pm 2) \times 10^{-5}$	308 ± 30
FCCM		
Radius (μm)		
10	$(3.6 \pm 1) \times 10^{-5}$	322 ± 9
20	$(8.6 \pm 2) \times 10^{-5}$	330 ± 3
40	$(4.8 \pm 1) \times 10^{-4}$	330 ± 3
60	$(1.3 \pm 0.07) \times 10^{-3}$	331 ± 2

Values listed are the average and standard deviation of a minimum of 12 measurements.

for the metal contacts, while the specific contact resistance between the metal and SiC was input separately. An electrical contact was defined on the top face of each cylinder.

An applied bias of 0.06 V was placed across the two contacts in the simulations. This voltage was similar to that imposed on the fabricated structures for the 0.1 mA current used in the experiments. The simulations utilized the materials parameters for SiC and Au included in the Sentaurus Device materials library along with the drift–diffusion model.[21] Two variables were manipulated to investigate the disparity between the FCCM and the other methods: the size of the outer contacts and the specific contact resistance. The size of the contacts was changed for different simulations, while adjusting a distributed resistance at the metal–SiC interface allowed us to adjust the specific contact resistance. The simulated contact radius and specific contact resistance ranged from 10 μm to 60 μm and 10^{-7} Ω cm^2 to 10^{-2} Ω cm^2, respectively. The specific contact and sheet resistance were then extracted for each case via the FCCM calculations using the simulated inner contact voltage drop and current.

A plot summarizing the results of the simulations is shown in Fig. 2. The accuracy of the specific contact resistance determined by the simulated FCCM structure was quantified by the ratio of the specific contact resistance from the simulated results to that input into the simulation, with 1 being the most accurate. The simulated results reveal the same trend observed in the fabricated structures, where for a given specific contact resistance, a smaller contact would deliver a more accurate result. Another interesting result from the simulations is that, as the defined specific contact resistance is increased, a higher degree of accuracy is provided for each contact size. Further investigation into these trends will be required to resolve the origin of the errors as well as supply guidelines to when the structure can be appropriately used.

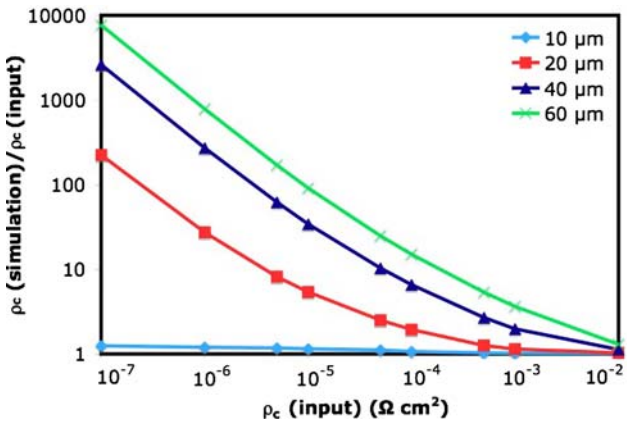

Fig. 2. Plot of the ratio of ρ_c determined from the simulations using the FCCM calculations to the input ρ_c as a function of the input ρ_c for various outer contact sizes.

Table II compares the experimental FCCM specific contact resistance values for different contact sizes from the fabricated structures (Table I) with the average value determined experimentally by the TLM and CTLM, 2.6×10^{-5} Ω cm^2, which is used as a baseline. Those values are compared with the ratio found by running a simulation using that average as the input specific contact resistance. The experimental and simulated ratios tend to agree. An important result from the simulations is that, using these materials and geometries, the FCCM will provide acceptable values of specific contact resistance in the range being investigated here.

RESULTS AND DISCUSSION

Good agreement in specific contact and semiconductor sheet resistance between the TLM, CTLM, and the FCCM using 10-μm-radius contacts is shown in Table I for the unstressed Ni contacts. Table III shows the change in specific contact resistance after different applied currents, as measured by the 10-μm-radius FCCM structures. The time to degradation was defined when the applied

Table II. Ratio of ρ_c Determined Experimentally by the FCCM (Simulated or Samples from Table I) for Different Contact Sizes to ρ_c Averaged from the CTLM and TLM in Table I, Used as a Baseline

	ρ_c (Experimental)/ρ_c (CTLM, TLM Avg.)			
	10 μm	**20 μm**	**40 μm**	**60 μm**
Simulated	1.2	3.4	16	42
Samples	1.4	3.3	18	50

Table III. Examples of the Change in Specific Contact Resistance at Different Currents Showing a Variation in Time and Current Needed for Degradation

Stressed Current (mA)	Time to Degradation (min)	Change in ρ_c (%)
400	>1 h	51
400	>1 h	9
400	0.25	460
400	10	650
500	>1 h	−50
500	Instantaneous	510
500	1.0	4100
500	23	2300
600	Instantaneous	410
600	0.10	2600
600	10	12000
750	Instantaneous	2400
750	Instantaneous	500
750	25	4600
750	36	5700

voltage increased to a 10 V compliance, which was typically followed by a sharp decrease in current. The increase in voltage was usually abrupt, with a change between 2 V and 3 V over a few seconds. The corresponding drop in current was also significant, declining to less than half the initial applied current. Entries marked "> 1 h" denote a stable contact with little or no increase in voltage over time to sustain the applied current, while "instantaneous" degradation occurred as soon as the current was applied. There was a large variability in time and current needed for degradation, with only about 15% of the contacts showing no degradation and about half failing instantly or within the first 30 s under various currents. Contacts that showed no degradation exhibited either a slight decrease or increase in specific contact resistance, keeping within one standard deviation of the average, while degraded contacts showed an order of magnitude or more increase. There was no significant change in sheet resistance in any of the structures.

The degraded contacts typically exhibited a stark contrast in appearance under optical microscope during the stressing. As soon as failure occurred, the bond pad above the contact changed from a smooth appearance to a mounded shape with observable cracking. FESEM revealed that the alteration in appearance was due to a significant change in surface morphology, as shown in Fig. 3, with a dome-like feature directly above the contact and cracking in the Au overlayer. To further investigate the source of this occurrence, cross sections of individual contacts were made using a FIB to mill a trench in the sample. Figure 4 shows FESEM micrographs of an unstressed and a degraded contact. The presence of voids is similar to that reported in other studies, where Kirkendall voids were observed in the Ni/SiC reaction region after annealing.[14–16] The large change in surface morphology can be attributed to the growth of voids, likely due to stresses from the high current density and Joule heating. Large void growth would reduce the active area of the contact, requiring an increase in applied voltage to sustain a constant current through the device. The variability in time to degradation and the current needed to degrade the contacts might be explained by a variation in the size or density of voids across all the Ni contacts.

Further analysis by AES was performed by selectively etching all the metal layers except the Ni/SiC reaction layer by using a series of wet etchants as mentioned previously. The SEM micrograph from the AES instrument (Fig. 5) shows a degraded contact with contrasting areas. The darker areas exhibited a relatively low Ni-to-Si signal, whereas the Ni signal in the lighter areas corresponded to an expected nickel silicide reaction product from the ohmic contact anneal. In comparison, the unstressed contacts were uniform with a strong Ni signal across the entire contact after undergoing the same etching conditions. The lack of Ni in areas of the stressed contacts can be explained by the large extent of void growth shown in Fig. 4, which could cause cracking in the film. The unattached layer could then be washed away during the wet-etching process, leaving only a part of the reaction layer behind. This is further evidence that growth of voids in the Ni/SiC reaction region is the failure mechanism for high-current-density stressing.

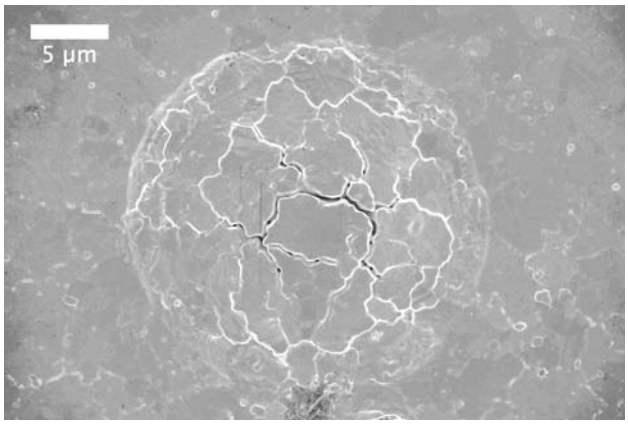

Fig. 3. FESEM micrograph of the top of the Au overlayer of a failed contact, showing a large change in surface morphology.

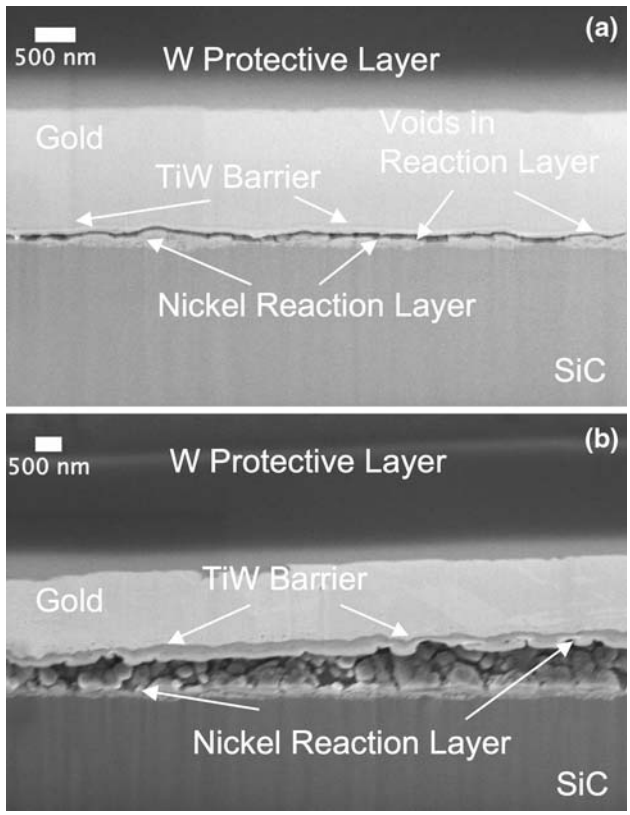

Fig. 4. FESEM micrograph of a sectioned (a) unstressed contact and (b) degraded contact showing void progression in the Ni reaction layer.

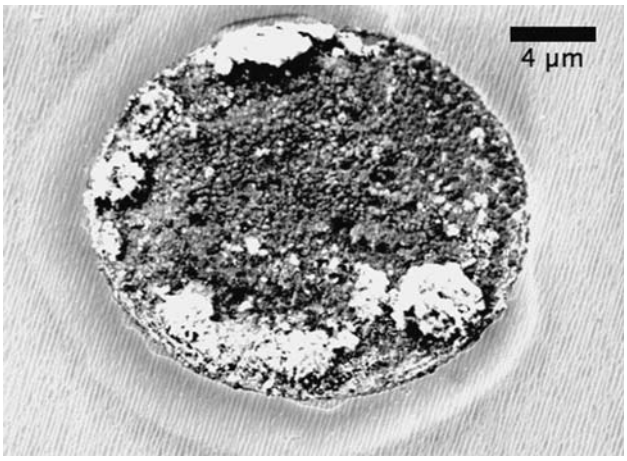

Fig. 5. SEM micrograph of a degraded contact with only the Ni/SiC reaction layer and SiC present.

It should be noted that vertical stressing leads to current flow through the entire area of the contact, and materials characterization revealed degradation over the entire contact. If nonuniform degradation were to occur, however, a lateral contact resistance measurement technique such as the FCCM would be more sensitive to degradation around the periphery of the contact than the center. The magnitude of this effect would depend on the size of the contact and the transfer length, which is a measure of the current crowding at the edge of the contact when current is transported laterally.

CONCLUSIONS

This study has presented a reliability test structure adapted from the FCCM that facilitates vertical current stressing of ohmic contacts and provides a means for electrically characterizing the contacts before and after stressing. By utilizing both fabricated test structures and simulations, the FCCM has been shown to provide acceptable values of specific contact and semiconductor sheet resistance using a 10-μm-radius contact, for this set of experiments, as validated by comparing the measured results with those from the CTLM and TLM. Functionality of the structure was illustrated through the high-current-density stressing of Ni ohmic contacts to a SiC PiN device. Growth of voids in the Ni/SiC reaction layer, as mentioned in previous studies, was revealed to be the cause of contact degradation at current densities exceeding 10^5 A/cm^2, established using FESEM of FIB-cut cross sections and AES. The disparity in time and current needed for degradation suggests nonuniform void formation among the contacts across the samples. Future work will entail the examination of other contact schemes to SiC in order to study other possible degradation mechanisms as well as any polarity effects.

ACKNOWLEDGEMENTS

This work was supported by the Office of Naval Research under Contract N00014-05-D-0275 DO-0002 and through the use of facilities at the Pennsylvania State University Materials Research Institute Nano Fabrication Network under the National Science Foundation Cooperative Agreement No. 0335765, National Nanotechnology Infrastructure Network, with Cornell University.

REFERENCES

1. J.S. Huang, K.N. Tu, S.W. Bedell, W.A. Lanford, S.L. Cheng, J.B. Lai, and L.J. Chen, *J. Appl. Phys.* 82, 2370 (1997). doi:10.1063/1.366047.
2. J.S. Huang, H.K. Liou, and K.N. Tu, *Phys. Rev. Lett.* 76, 2346 (1996). doi:10.1103/PhysRevLett.76.2346.
3. K.N. Chen, H.H. Lin, S.L. Cheng, Y.C. Peng, G.H. Shen, L.J. Chen, C.R. Chen, J.S. Huang, and K.N. Tu, *J. Mater. Res.* 14, 4720 (1999). doi:10.1557/JMR.1999.0639.
4. C.C. Lin, W.S. Chen, H.L. Hwang, K.Y.J. Hsu, H.K. Liou, and K.N. Tu, *Appl. Surf. Sci.* 92, 660 (1996). doi:10.1016/0169-4332(95)00314-2.
5. L.J. Chen, K.N. Chen, H.H. Lin, S.L. Cheng, Y.C. Peng, G.H. Shen, and C.R. Chen, *International Conference on Ion Implantation Technology Proceedings*, Vol. 2 (1999), p. 837.
6. L.-Z. Chen and K.Y.-J. Hsu, *Solid-State Electron.* 43, 1031 (1999). doi:10.1016/S0038-1101(99)00020-9.
7. S. Vaidya, R.J. Schutz, and A.K. Sinha, *J. Appl. Phys.* 55, 3514 (1984). doi:10.1063/1.332940.
8. J.B. Casady and R.W. Johnson, *Solid-State Electron.* 39, 1409 (1996). doi:10.1016/0038-1101(96)00045-7.
9. J. Crofton, P.G. McMullin, J.R. Williiams, and M.J. Bozack, *J. Appl. Phys.* 77, 1317 (1994). doi:10.1063/1.358936.
10. S.Y. Han, J.-Y. Shin, B.-T. Lee, and J.-L. Lee, *J. Vac. Sci. Technol. B* 20, 1496 (2002). doi:10.1116/1.1495506.
11. I.P. Nikitina, K.V. Vassilevski, N.G. Wright, A.B. Horsfall, A.G. O'Neill, and C.M. Johnson, *J. Appl. Phys.* 97, 083709 (2005). doi:10.1063/1.1872200.
12. L.G. Fursin, J.H. Zhao, and M. Weiner, *Electron. Lett.* 37, 1092 (2001). doi:10.1049/el:20010738.
13. C.M. Eichfeld, M.A. Horsey, S.E. Mohney, A.V. Adedeji, and J.R. Williams, *Thin Solid Films* 485, 207 (2005). doi:10.1016/j.tsf.2005.04.005.
14. M.W. Cole, P.C. Joshi, C.W. Hubbard, M.C. Wood, M.H. Ervin, B. Geil, and F. Ren, *J. Appl. Phys.* 88, 2652 (2000). doi:10.1063/1.1287776.
15. Ts. Marinova, A. Kakanakova-Georgieva, V. Krastev, R. Kakanakov, M. Neshev, L. Kassamakova, O. Noblanc, C. Arnodo, S. Cassette, C. Brylinski, B. Pecz, G. Radnoczi, and Gy. Vincze, *Mater. Sci. Eng. B* 46, 223 (1997). doi:10.1016/S0921-5107(96)01981-2.
16. B. Pecz, *Appl. Surf. Sci.* 184, 290 (2001). doi:10.1016/S0169-4332(01)00678-X.
17. S.J. Chua and S.H. Lee, *Solid-State Electron.* 35, 1331 (1992). doi:10.1016/0038-1101(92)90168-C.
18. K. Dieter, *Shroder, Semiconductor Material and Device Characterization*, 2nd ed. (New York: Wiley, 1998), p. 156.
19. G.M. Marlow and M.B. Das, *Solid-State Electron.* 25, 91 (1982). doi:10.1016/0038-1101(82)90036-3.
20. W. Kern and D.A. Puotinen, *RCA Rev.* 31, 187 (1970).
21. *Synopsys Sentaurus Device User's Manual: Release Z-2007.03* (Synopsys, Inc., 2007).